CHALMERS
UNIVERSITY OF TECHNOLOGY

Low-field mobility and high-field velocity of charge carriers in InGaAs/InP high-electron-mobility transistors

Downloaded from: https://research.chalmers.se, 2026-04-05 21:06 UTC

Citation for the original published paper (version of record):
Harrysson Rodrigues, I., Vorobiev, A. (2022). Low-field mobility and high-field velocity of charge carriers in InGaAs/InP
high-electron-mobility transistors. IEEE Transactions on Electron Devices, 69(4): 1786-1791.
http://dx.doi.org/10.1109/TED.2022.3147733

N.B. When citing this work, cite the original published paper.

© 2022 IEEE. Personal use of this material is permitted. Permission from IEEE must be obtained for all other uses, in any current or future media, including reprinting/republishing this material for advertising or promotional purposes, or reuse of any copyrighted component of this work in other works.

(article starts on next page)

Low-field mobility and high-field velocity of charge carriers in InGaAs/InP high-electron-mobility transistors

Isabel Harrysson Rodrigues, Andrei Vorobiev
Department of Microtechnology and Nanoscience,
Chalmers University of Technology,
SE-41296 Gothenburg, Sweden
{isabelr@chalmers.se}

***Abstract*—Development of transistors for advanced low noise amplifiers requires better understanding of mechanisms governing the charge carrier transport in correlation with the noise performance. In this paper, we report on study of the carrier velocity in InGaAs/InP high-electron-mobility transistors (HEMTs) found via geometrical magnetoresistance in the wide range of the drain fields, up to 2 kV/cm, at cryogenic temperature of 2 K. We observed, for the first time experimentally, the velocity peaks and found that the peak velocity and corresponding field decrease significantly with the transverse field. The low-field mobility and peak velocity are found to be up to 65000 cm^2/Vs and 1.2$\times$10^6 cm/s, respectively. Extrapolations to the lower transverse fields show that the peak velocity can be as high as 2.7$\times$10^7 cm/s. The corresponding intrinsic transit frequency can be up to 172 GHz at the gate length of 250 nm. We demonstrated, for the first time, that the low-field mobility and peak velocity reveal opposite dependencies on the transverse field, indicating the difference in carrier transport mechanisms dominating at low- and high-fields. Therefore, the peak velocity is an appropriate parameter for characterization and development of the low noise HEMTs, complementary to the low-field mobility. Analysis indicates that the low-field carrier transport is governed by screening of the Coulomb potential of ionized impurities responsible for the carrier scattering. The velocity overshoot is associated with the electron quantization and subband formation caused by the transverse field. The results of the research clarify the ways of the further development of the HEMTs for advanced applications.**

I. Introduction

High-electron-mobility transistors (HEMTs) have long been the transistor of choice for extremely low-noise amplifiers (LNAs) operating in microwave and millimeter wave bands due to their superior noise and gain performance [1]. Cryogenic LNAs based on state-of-the-art InGaAs/InP HEMTs provide outstanding performance thanks to ultra-high carrier mobility and velocity [2, 3]. Important applications range from cryogenic read out circuits for quantum computing [4] to surveillance [5] and radio astronomy [6]. The performance of LNAs is defined by the amplifier gain and noise figure related to fluctuations of carrier velocity and concentration [7]. It has been shown theoretically, that the noise figure is inversely proportional to the transit frequency, i.e. velocity of the charge carriers [8]. Experimentally, the lowest noise figure is observed at drain fields corresponding to the beginning of the drain current saturation region [9]. To further improve the HEMT technology, it is important to clarify the mechanisms governing the charge carrier transport.

The charge carrier transport in bulk InGaAs has been studied theoretically, and a model for GaAs and other materials with a similar band structure has been published [10]. A recent publication presents an evaluation of the electric field dependent drift velocity in the ultra-thin films of $In_{0.53}Ga_{0.47}As$ using Monte Carlo simulations [11]. However, there are no previous publications on carrier velocity in InGaAs/InP HEMTs studied theoretically or experimentally, especially at cryogenic temperatures.

Already in the early years of the HEMTs development it has been proposed that the carrier mobility and velocity can be found and studied using geometrical magnetoresistance (gMR) method [12, 13]. The gMR effect arises when the magnetic field causes the path of the charge carriers to deviate from a straight line, raising the sample resistance [14]. An advantage of this method, in comparison with other methods of evaluation of the carrier velocity, is that it does not require knowledge of the carrier concentration or capacitance, the transistor gate length, access resistance and threshold voltage [15]. In particular, the methods of evaluation of the effective and field-effect mobility from the output and transfer characteristics usually approximate carrier concentration from the simple parallel-plate capacitance model, which may result in large errors. In contrary, the gMR method measures, and allows for analysis, the carrier velocity directly and, hence, more accurately. However, in spite of this obvious advantage, there are very limited number of publications on carrier velocity in HEMTs studied using the gMR. The dc and ac magnetoresistance measurements were used for analysis of the low-field mobility and quasi-ballistic charge carrier transport in Si MOSFETs and AlGaN/GaN HEMTs [15, 16]. The ac gMR method preserves the most important advantages of the original one, i.e. dc gMR method, while eliminating parasitic contribution of series resistance via modulation of the gate voltage by square pulses and measuring the derivative of the transistor resistance [15]. The method has been verified on modulation-doped test structures,

i.e. without an actual gate, using the channel composition of $Al_{0.30}Ga_{0.70}As$, which is different from that used in the modern HEMTs for LNAs, e.g. $In_{0.65}Ga_{0.35}As$. Moreover, the modern InGaAs HEMT LNAs operate at lower temperatures, below 10 K, whereas the experiments previously done were carried out at 77 K [12]. To the best of our knowledge, there are no publications on the carrier velocity in the modern InGaAs HEMTs studied using gMR.

In this work, we studied the low-field mobility and high-field velocity of the charge carriers in modern InGaAs/InP HEMTs in the range of the drain field up to velocity saturation, at cryogenic temperatures, using the gMR method and for different gate voltages applying a modified semi-empirical velocity model. This allowed for accurate evaluation of the charge carrier transport in InGaAs/InP HEMTs at the beginning of the drain source current saturation. We, in particular, demonstrate experimentally, for the first time, the velocity peaks in InGaAs/InP HEMTs and that the low-field mobility and high-field velocity reveal opposite dependencies on the transverse field.

II. Fabrication and Measurement Method

The devices used in this study, were dual-finger InGaAs/InP HEMTs, with the gate length $L = 250$ nm and the total gate width $W = 100$ μm. We deliberately selected HEMTs having a relatively large gate length with the goal to minimize quasi-ballistic transport effects by keeping the gate longer than the mean free path of the charge carriers, which one can consider as a limitation of the work [16, 17]. The devices were fabricated using a conventional top-down approach, planar lithography and wet etching of an InGaAs/InP based heterostructure [18]. These type of HEMTs reveal excellent noise performance with minimum noise temperature down to 1 K [19]. The heterostructure stack, grown by molecular beam epitaxy, consists, from top to bottom, of a 20 nm thick $In_{0.53}Ga_{0.47}As$ cap layer doped to a Si concentration of 5×10^{19} cm^{-3}, an 11 nm thick $In_{0.52}Al_{0.48}As$ barrier, a 5×10^{12} cm^{-2} Si delta doping, a 3 nm thick $In_{0.52}Al_{0.48}As$ spacer, a 15 nm thick $In_{0.65}Ga_{0.35}As$ channel, and a 500 nm thick $In_{0.52}Al_{0.48}As$ buffer, on top of a semi-insulating InP layer with thickness of 75-100 μm.

The mesa was prepared using laser lithography, chemical wet etching and photoresist stripping. The ohmic contacts consisting of an nickel-germanium-gold alloy were prepared by electron-beam lithography, oxide removal and metal deposition, followed by lift-off and rapid thermal annealing. The gate was exposed using electron beam lithography, followed by gate recess, oxide removal and metal deposition, then lift-off. The gate material used was titanium, platinum and gold. Larger pads, for adhesion purposes were added through laser lithography, oxide removal, metal deposition and lift-off.

Fig. 1 shows two scanning electron microscopy images of the top- and side views of the fabricated device with equivalent circuit of corresponding resistances. The resistances associated with the junctions (R_j) and ungated regions of the channel (R_{ung}) together constitute the series resistance $R = 2R_j + 2R_{ung}$. The total (extrinsic) drain resistance can, therefore, be expressed as $R_{DS} = R + R_{ds}$, where R_{ds} is the resistance of the gated region of the channel.

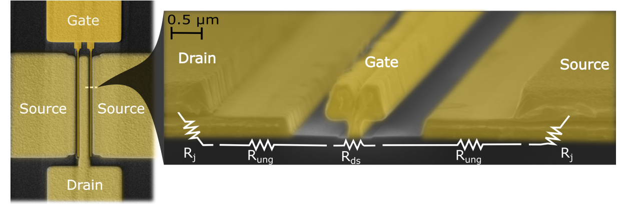

Figure 1. Scanning electron microscopy images of a dual-finger device and a zoom in on the cross-section of a gate area, where the metal contacts are highlighted in yellow, with equivalent circuit of corresponding resistances.

The dc measurements were carried out in a Quantum Design Physical Property Measurement System, providing a vacuum environment at a temperature of 2 K and under a static magnetic field of 0.4 T. The HEMT channel was placed perpendicular towards the applied magnetic field, hence giving rise to gMR. In short, the gMR effect occurs in samples with relatively low L/W ratios. In this case, the full Hall voltage is not developed to balance the Lorentz force, and carriers near the contacts move at an angle to the applied electric field. The longer path leads to higher resistance [14]. The gMR method is free from limitations inherent to other methods of mobility evaluation, in particular, it does not require knowing the carrier concentration nor assumption of constant mobility [14]. This allows for accurate evaluation and study of the mobility and velocity in real HEMTs, in the whole range of the drain and gate voltages.

III. Results and Discussion

Fig. 2 (a) shows typical output characteristics of HEMTs, i.e. the drain current (I_{DS}) versus extrinsic drain voltage (V_{DS}), measured in the common source configuration, at different extrinsic gate voltages (V_{GS}) varying from -0.2 V to 0.4 V with a step of 0.05 V with and without magnetic field. It can be seen that the drain current tends to saturate in the whole range of gate voltages. It can also be seen from Fig. 2 (a), that the drain current decreases with the magnetic field. According to the analysis made in our previous work, the observed variations in the drain current with the magnetic field are governed by the gMR effect and other possible sources of the drain current variations, including the measurement artefacts, can be neglected [18].

Fig. 2 (b) shows the transfer characteristics of the HEMT, i.e. the drain current versus extrinsic gate voltage, obtained from the output characteristics (shown in Fig. 2 (a)) with V_{DS} increasing in direction of arrow from 0.05 V to 0.35 V in steps of 0.05 V, with and without magnetic field. The threshold voltage is calculated as $V_T = V_{GS_0} - 0.5V_{DS}$, where V_{GS_0} is found by extrapolation of the linear parts of the transfer characteristics to $I_{DS} = 0$, as indicated by a straight line in Fig. 2 (b). Fig. 2 (c) shows the drain source resistance, calculated as $R_{DS} = V_{DS}/I_{DS}$, versus V_{GS} at different V_{DS}

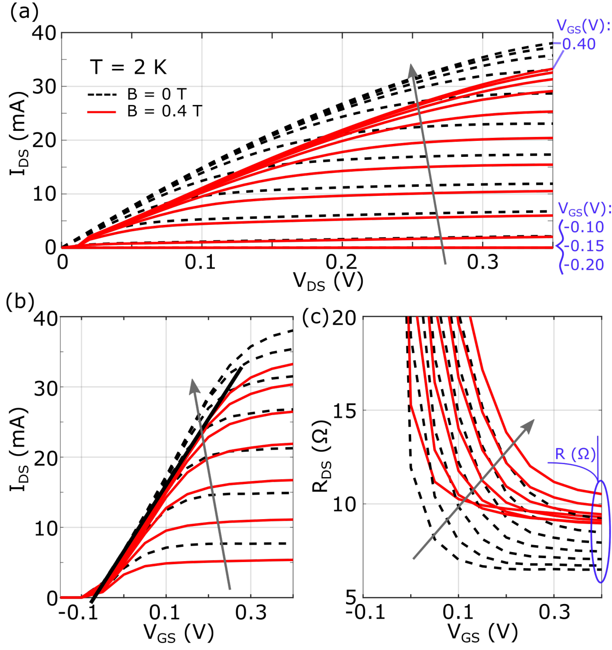

Figure 2. DC characteristics of the InGaAs/InP HEMT measured at 2 K with (solid red lines) and without (black dashed lines) magnetic field. a) Output characteristics at different extrinsic gate voltages varying in direction of arrow from -0.2 V to 0.4 V with a step of 0.05 V. b) Transfer characteristics at different extrinsic drain voltages varying in direction of arrow from 0.05 V to 0.35 V with a step of 0.05 V. The black solid line represents an extrapolation of a dependence to $I_{ds} = 0$ for evaluation of the threshold voltage. c) Drain source resistance R_{DS} versus extrinsic gate voltage at different drain voltages varying in direction of arrow from 0.05 V to 0.35 V with a step of 0.05 V. The total series resistance R is reached once R_{DS} resistance versus V_{GS} saturates.

with and without magnetic field. It can be seen that, at high enough V_{GS}, the R_{DS} tends to be nearly independent on the gate voltage. The similar dependencies were observed in AlGaN HEMTs and explained by that at high V_{GS}, i.e. high carrier concentration in gated region, the R_{ds} becomes negligible compared to R [20, 21]. We assume that there is no significant effect of inducing the carriers into the conduction band minimum caused by lowering the quasi-Fermi level down to conduction band at high gate voltages [22]. We assume also that the low-field mobility is not degraded with the gate voltage. In contrary, one can expect increase in the low-field mobility due to screening of Coulomb potential of impurities [23, 24]. Therefore, the saturation of the R_{DS} dependencies at higher V_{GS} can be explained mainly by the R dominating over the R_{ds}. These allows us to evaluate the series resistance as $R = R_{DS}$ at $V_{GS} = 0.4$ V. Analysis of fitting curves to the dependencies of R_{DS} on V_{GS}, shown in Fig. 2 (c), indicates, that error in evaluation of R, using this approach, is less than 3 % in the whole range of V_{DS}, with and without magnetic field. One can conclude from Fig. 2 (c), that the series resistance depends on both electric and magnetic fields. The increase in the series resistance with magnetic field can be explained by the gMR effect in the ungated regions of the channel. The increase in the series resistance with the lateral electric field can be explained by the velocity overshoot and saturation of the velocity of the

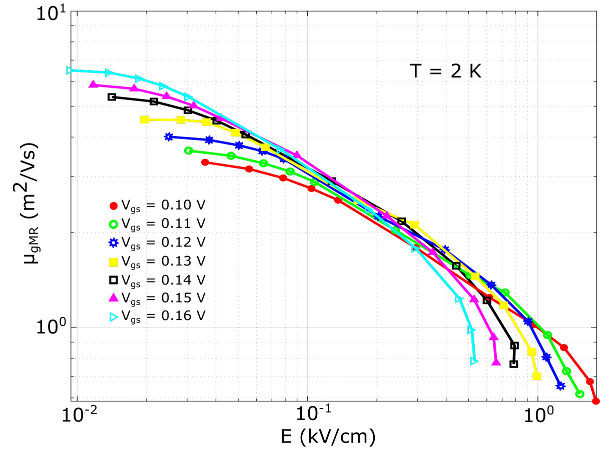

Figure 3. Geometrical magnetoresistance mobility (μ_{gMR}) versus intrinsic drain field (E) at different intrinsic gate voltages (V_{gs}), at 2 K.

charge carriers in the ungated regions [25], which is confirmed in the following analysis.

As it can be seen from Fig. 2 (c), the series resistance contributes significantly or even dominates in the extrinsic drain resistance in the studied ranges of the extrinsic gate and drain voltages. Therefore, for correct analysis of the charge carrier transport, we introduce intrinsic gate and drain voltages, (V_{gs}) and (V_{ds}) respectively, calculated as [26]

$$V_{gs} = V_{GS} - I_{ds}\frac{R}{2} \tag{1}$$

$$V_{ds} = V_{DS} - I_{ds}R \tag{2}$$

Calculations using Eqs. (1)-(2) show that the intrinsic gate overdrive voltage, i.e. $V_{gs} - V_T$, varies in the range of 0.16-0.22 V, which is sufficiently larger than the largest applied intrinsic drain voltage of 0.05 V. This allows us to ignore effects associated with depletion of the charge carriers at the drain side caused by the gate-drain voltage.

The gMR mobility is calculated as

$$\mu_{gMR} = \frac{1}{B}\sqrt{\frac{R_{ds}^B}{R_{ds}^0} - 1}, \tag{3}$$

where B is the magnetic flux density, R_{ds}^B and R_{ds}^0 are the resistances of the gated region of the channel calculated as ratios between the intrinsic drain voltage, found using Eq. (2), and the drain current, i.e. V_{ds}/I_{ds}, with and without magnetic field, respectively. Fig. 3 shows the μ_{gMR} versus intrinsic drain field, calculated as $E = \frac{V_{ds}}{L}$, at different intrinsic gate voltages varying in the range 0.10 V-0.16 V. The values of the low-field mobility agree well with that of 60000 cm^2/Vs found by Hall effect in the InGaAs heterostructures with approximately similar composition [27, 28].

It can be seen from Fig. 3, that there are two regions of the intrinsic drain field, below and above of approximately 0.2 kV/cm, with opposite dependencies of the mobility on the gate voltage. The mobility increases with the gate voltage at lower fields, while it decreases at higher fields. Therefore, one

can conclude that at the correspondingly lower and higher fields the charge carrier transport is governed by different mechanisms. This agrees well with the results of the experimental studies of the AlGaAs-GaAs modulation-doped structures, which showed that higher low-field mobility does not lead to a higher high-field velocity [13]. The possible mechanisms governing the charge carrier transport at low- and high-fields will be discussed below.

Fig. 4 shows the effective drift velocity of the charge carriers calculated as [29]

$$v = \mu_{gMR} \times E \tag{4}$$

versus intrinsic drain field at different intrinsic gate voltages. At relatively high intrinsic drain fields, above 0.3 kV/cm, the velocity peaks can be clearly seen. To the best of our knowledge, this is the first direct experimental observation of the velocity peaks in the InGaAs HEMTs. The velocity peaks in the ultra-thin films of $In_{0.53}Ga_{0.47}As$ were predicted by Monte Carlo simulations [11]. However, for example, the earlier experimental studies of the AlGaAs-GaAs modulation-doped structures did not reveal the velocity peaks [13]. As it can be seen from Fig. 4, the peak velocity (v_{peak}) and corresponding field (E_{peak}) are strongly dependent on the gate voltage, i.e. transverse field, both decreasing with increased V_{gs}. The velocity overshoot indicates that the drift velocity and field are distributed along the channel [30]. Therefore, the velocity calculated using Eq. (4) and respective drain field represent corresponding effective values.

Our analysis has shown that the drift velocity models developed for bulk GaAs [10] results in a significant overestimation of the velocity and does not reproduce the shape of the dependencies accurately. Better agreement can be achieved by using a semi-empirical model originally developed for AlGaN HEMTs [31, 32] modified as

$$v = \frac{\mu_0 E + v_{sat}\left(\frac{E}{E_T}\right)^k}{1 + \left(\frac{E}{E_T}\right)^k + a\left(\frac{E}{E_T}\right)} \tag{5}$$

where the low-field mobility (μ_0), saturation velocity (v_{sat}), transfer field (E_T),and coefficients a and k are used as fitting parameters. Here a and k define the velocity overshoot and the width of the velocity peak, respectively [32]. The lines in Fig. 4 represent the velocity calculated using Eq. (5) for different intrinsic gate voltages.

Table I contains the parameters at different intrinsic gate voltages. It is clear that the transfer field and coefficients a and k reveal monotonous dependencies versus intrinsic gate voltage. It can be seen, from Table I and Fig. 4, that the transfer field is typically slightly larger than the corresponding peak field.

The effective carrier concentration in the gated region can be estimated as [14]

$$n = C_g \frac{(V_{gs} - V_T)}{q}, \tag{6}$$

where q is the elementary charge and $C_g = \frac{\epsilon \times \epsilon_0}{d}$ is the gate capacitance per unit area, where $d = 14$ nm and $\epsilon \approx 13$ are the total thickness and the effective dielectric constant of the

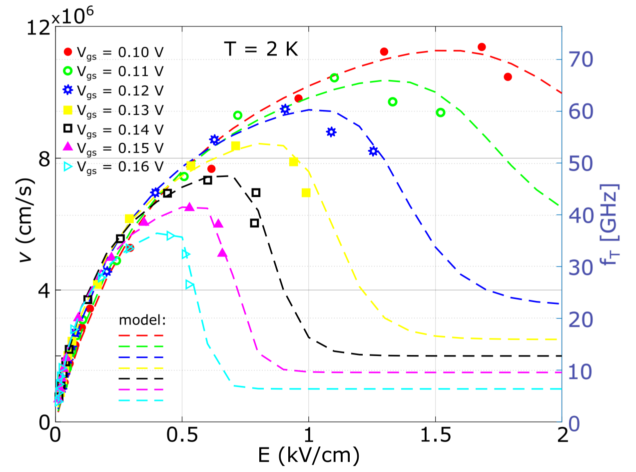

Figure 4. Effective drift velocity (v) and corresponding intrinsic transit frequency (f_T) versus intrinsic drain field (E) at different intrinsic gate voltages (V_{gs}), at 2 K. The lines represent dependencies calculated using Eq. (5).

barrier and spacer layers, and ϵ_0 the dielectric constant for vacuum [18, 33].

Fig. 5 shows the low-field mobility found using the model presented by Eq. (5), and peak velocity found from Fig. 4, versus both intrinsic gate overdrive voltage and concentration, calculated by Eq. (6), of the charge carriers. Extrapolation of dependencies in Fig. 5 and Fig. 4 down to $V_{gs} - V_T = 0$ indicates that the peak velocity can be as high as 2.7×10^7 cm/s with corresponding peak field up to 4.4 kV/cm, which are in good agreement with those values simulated for ultra-thin InGaAs films [11]. The values of the low-field mobility agree well with those of μ_{gMR} shown in Fig. 3 extrapolated to low drain fields. Additionally, the low-field mobility of 65000 cm^2/Vs and concentration of $2{\times}10^{12}$ cm^{-2} found in our Hall effect measurements of the same structure as the InGaAs/InP HEMTs presented here agree well with those shown in Fig. 5, which, in particular, verifies our methods of evaluation of the mobility and carrier concentration.

Fig. 5 demonstrates clearly that the low-field mobility and peak velocity reveal opposite dependencies on the gate voltage. This agrees with the results of the earlier studies of the carrier velocity in MODFETs showed that the higher low-field mobility does not lead to a higher high-field velocity [13]. One can explain it by the different mechanisms governing the charge carrier transport at the low and high fields. Therefore, the peak velocity is an appropriate parameter for characterization and development of the low noise HEMTs, complementary to the typically used low-field mobility.

The similar increase in the low-field mobility with the gate voltage, in the corresponding range of the carrier concentration, have been observed in a number of experiments in the InGaAs HEMTs and MOSFETs [34–38]. The increase of the low-field mobility with the carrier concentration is explained by increased screening of the Coulomb potential of the ionized impurities responsible for the carrier scattering [23, 24].

Table I
PARAMETERS USED FOR FITTING THE DEPENDENCIES OF THE DRIFT VELOCITY ON INTRINSIC DRAIN FIELD, SHOWN IN FIG. 4, BY THE SEMI-EMPIRICAL MODEL GIVEN BY EQ. (5).

V_{gs} (V)	μ_0 (cm^2/Vs)	v_{peak} (cm/s)	E_T (kV/cm)	v_{sat} (cm/s)	a	k
0.10	32000	1.1×10^7	1.8	7.0×10^6	3.4	10
0.11	36000	1.0×10^7	1.5	6.0×10^6	3.6	12
0.12	40000	9.6×10^6	1.2	4.0×10^6	3.9	13
0.13	45000	8.4×10^6	0.9	3.0×10^6	4.0	15
0.14	54000	7.3×10^6	0.7	2.0×10^6	4.3	16
0.15	58000	6.5×10^6	0.6	1.5×10^6	4.5	18
0.16	65000	5.7×10^6	0.5	1.0×10^6	4.6	20

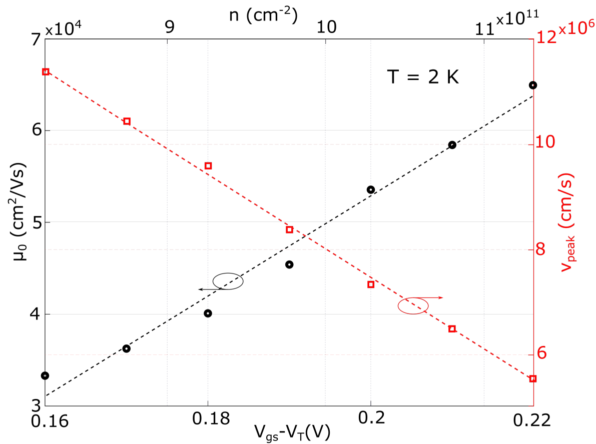

Figure 5. Low-field mobility (μ_0) and peak velocity (v_{peak}) versus intrinsic gate overdrive voltage ($V_{gs} - V_T$) and corresponding concentration of the charge carriers (n), at 2 K.

The observed decreases in the v_{peak} and E_{peak}, with the intrinsic gate voltage, see Fig. 4 and Fig. 5, are, most likely, associated with the electron quantization and sub-band formation caused by the transverse field. According to the model of the electron quantization, the sub-band energies are proportional to the transverse electric field [39–42]. Therefore, one can expect a change in proportion of carriers in the upper valleys, which exhibit a higher effective mass at higher energies due to the band structure of InGaAs and consequently a corresponding decrease in the drift velocity, with higher gate voltages.

The curves in Fig. 4 also shows the intrinsic transit frequency calculated as $f_T = \frac{v}{2\pi L}$ [29]. The peak velocity of 2.7×10^7 cm/s, found by extrapolation of the dependence in Fig. 5 to $V_{gs} - V_T = 0$, corresponds to $f_T = 172$ GHz, which is in very good agreement with the transit frequencies of the state-of-the-art InP HEMTs [43]. This further validates the proposed method of the carrier velocity evaluation using the gMR mobility.

IV. CONCLUSION AND OUTLOOK

In conclusion, we used the geometrical magnetoresistance method for study of the carrier velocity in the InGaAs/InP HEMTs, developed for advanced LNAs, in the wide range of the drain fields, up to 2 kV/cm, at cryogenic temperature of 2 K. We observed, for the first time experimentally, the velocity peaks in the InGaAs/InP HEMTs with peak velocity, up to 1.2×10^6 cm/s, and corresponding field decreasing significantly with the transverse field. We demonstrated, also for the first time, that the low-field mobility and peak velocity reveal opposite dependencies on the transverse field, indicating the difference in carrier transport mechanisms dominating at low- and high-fields. Therefore, the peak velocity is an appropriate parameter for characterization and development of the low noise HEMTs, complementary to the low-field mobility. These findings can play an important role in further development of the high performance HEMTs, in particular, for applications in the LNAs. In the future work, we plan to apply the gMR method for analysis of the InGaAs/InP HEMTs with different gate length, down to 60 nm, with the aim to study quasi-ballistic charge carrier transport.

ACKNOWLEDGMENT

This work was performed in part at Myfab Chalmers. The authors also thank Professors Jan Stake, Jan Grahn, Kjell Jeppson, Niklas Rorsman, Associate Professor Helena Rodilla and Docent Hans Hjelmgren for fruitful discussions.

REFERENCES

[1] K. M. K. H. Leong, X. Mei, W. Yoshida, P. Liu, Z. Zhou, M. Lange, L. Lee, J. G. Padilla, A. Zamora, B. S. Gorospe, K. Nguyen, and W. R. Deal, "A 0.85 THz Low Noise Amplifier Using InP HEMT Transistors," *IEEE Microw. Wirel. Compon. Lett.*, vol. 25, no. 6, p. 397, 2015.
[2] E. Cha, N. Wadefalk, P.-A. Nilsson, J. Schleeh, G. Moschetti, A. Pourkabirian, S. Tuzi, and J. Grahn, "0.3–14 and 16–28 ghz wide-bandwidth cryogenic mmic low-noise amplifiers," *IEEE Transactions on Microwave Theory and Techniques*, vol. 66, no. 11, pp. 4860–4869, 2018.
[3] E. Cha, N. Wadefalk, G. Moschetti, A. Pourkabirian, J. Stenarson, and J. Grahn, "Inp hemts for sub-mw cryogenic low-noise amplifiers," *IEEE Electron Device Letters*, vol. 41, no. 7, pp. 1005–1008, 2020.
[4] J. C. Bardin, D. H. Slichter, and D. J. Reilly, "Microwaves in Quantum Computing," *IEEE J. Microwaves*, vol. 1, no. 1, p. 403, 2021.
[5] R. Appleby, R. Anderton, "Millimeter-wave and submillimeter-wave imaging for security and surveillance." *Proc. IEEE*, vol. 95, p. 1683, 2007.
[6] W. Ciccognani, E. Limiti, P. E. Longhi, and M. Renvoise, "Mmic lnas for radioastronomy applications using advanced industrial 70 nm metamorphic technology." *IEEE J. Solid-State Circuits*, vol. 45, p. 2008, 2010.
[7] C. A. Liechti, "Microwave field-effect transistors - 1976," *IEEE Trans. Microw. Theory Tech.*, vol. 24, no. 6, p. 279, 1976.
[8] M. W. Pospieszalski, "Modeling of noise parameters of MESFETs and MODFETs and their frequency and temperature dependence," *IEEE Trans. Microw. Theory Tech.*, vol. 37, no. 9, p. 1340, 1989.
[9] B. U. H. Klepser, C. Bergamaschi, M. Schefer, C. G. Diskus, W. Patrick, and W. Bachtold, "Analytical Bias Dependent Noise Model for InP HEMT's," *IEEE Trans. Electron Devices*, vol. 42, no. 11, p. 1882, 1995.
[10] J. Barnes, R. Lomax, and G. Haddad, "Finite-element simulation of gaas mesfets with lateral doping profiles and submicron gates," *IEEE Trans. on Electron Devices*, vol. 23, no. 9, p. 1042, 1976.
[11] E. Caruso, A. Pin, P. Palestri, and L. Selmi, "On the electron velocity-field relation in ultra-thin films of III-V compound semiconductors for advanced CMOS technology nodes," *Joint International EUROSOI Workshop and International Conference on Ultimate Integration on Silicon-ULIS, EUROSOI-ULIS 2017 - Proceedings*, p. 152, 2017.
[12] W. T. Masselink, W. Kopp, T. Henderson, and H. Morkoç, "Measurement of the Electron Velocity-Field Characteristic in Modulation-Doped Structures Using the Geometrical Magnetoresistance Method," *IEEE Electron Device Lett.*, vol. 6, no. 10, p. 539, 1985.
[13] W. T. Masselink, T. S. Henderson, J. Klem, W. F. Kopp, and H. Morkoc, "Dependence of 77 K electron velocity-field characteristics on low-field

mobility in AlGaAs-GaAs modulation-doped structures." *IEEE Trans. Electron Devices*, vol. ED-33, no. 5, p. 639, 1986.
[14] D. K. Schroder, *Semiconductor Material and Device, Third Edition*. Wiley-IEEE Press, 2006.
[15] M. Sakowicz, R. Tauk, J. Łusakowski, A. Tiberj, W. Knap, Z. Bougrioua, M. Azize, P. Lorenzini, K. Karpierz, and M. Grynberg, "Low temperature electron mobility and concentration under the gate of AlGaN/GaN field effect transistors," *Journal of Appl. Phys.*, vol. 100, no. 11, 2006.
[16] J. Łusakowski, W. Knap, Y. Meziani, J. P. Cesso, A. El Fatimy, R. Tauk, N. Dyakonova, G. Ghibaudo, F. Boeuf, and T. Skotnicki, "Electron mobility in quasi-ballistic Si MOSFETs," *Solid-State Electronics*, vol. 50, no. 4, p. 632, 2006.
[17] Jing Wang and M. Lundstrom, "Ballistic transport in high electron mobility transistors," *IEEE Trans. Electron Devices*, vol. 50, no. 7, p. 1604, 2003.
[18] I. H. Rodrigues, D. Niepce, A. Pourkabirian, G. Moschetti, J. Schleeh, T. Bauch, and J. Grahn, "On the angular dependence of InP high electron mobility transistors for cryogenic low noise amplifiers in a magnetic field," *AIP Advances*, vol. 9, no. 8, p. 085004, 2019.
[19] J. Schleeh, G. Alestig, J. Halonen, A. Malmros, B. Nilsson, P. A. Nilsson, J. P. Starski, N. Wadefalk, H. Zirath, and J. Grahn, "Ultralow-Power Cryogenic InP HEMT With Minimum Noise Temperature of 1 K at 6 GHz," *IEEE Electron Device Lett.*, vol. 33, no. 5, p. 664, 2012.
[20] X. Liu, Y. Lu, W. Yu, J. Wu, J. He, D. Tang, Z. Liu, P. Somasuntharam, D. Zhu, W. Liu, P. Cao, S. Han, S. Chen, and L. S. Tan, "Algan/gan metal-oxide-semiconductor high-electron-mobility transistor with polarized p(vdf-trfe) ferroelectric polymer gating," *Sci. Rep.*, vol. 5, no. nr 14092, 2015.
[21] X. F. Zhang, L. Wei, L. Wang, J. Liu, and J. Xu, "Gate length related transfer characteristics of gan-based high electron mobility transistors," *Appl. Phys. Lett.*, vol. 102, 3 2013.
[22] M. Shur and T. A. Fjeldly·, *Compound Semiconductor Device Modelling*. Springer-Verlag London Limited, 1993, no. pp. 56-73.
[23] M. E. Levinshtein, P. A. Ivanov, M. A. Khan, G. Simin, J. Zhang, X. Hu, and J. Yang, "Mobility enhancement in AlGaN/GaN metal-oxide-semiconductor heterostructure field effect transistors," *Semicond Sci Technol.*, vol. 18, no. 7, p. 666, jun 2003.
[24] M. Marso, J. Bernát, P. Javorka, and P. Kordoš, "Influence of a carrier supply layer on carrier density and drift mobility of AlGaN/GaN/SiC high-electron-mobility transistors," *Appl. Phys. Lett.*, vol. 84, no. 15, p. 2928, 2004.
[25] T. Palacios, S. Rajan, A. Chakraborty, S. Heikman, S. Keller, S. P. DenBaars, and U. K. Mishra, "Influence of the dynamic access resistance in the gm and f t linearity of algan/gan hemts," *IEEE Trans. Electron Devices*, vol. 52, p. 2117, 10 2005.
[26] A. Ortiz-Conde, A. Sucre-González, F. Zárate-Rincón, R. Torres-Torres, R. S. Murphy-Arteaga, J. J. Liou, and F. J. García-Sánchez, "A review of DC extraction methods for MOSFET series resistance and mobility degradation model parameters," *Microelectronics Reliability*, vol. 69, pp. 1–16, 2017. [Online]. Available: http://dx.doi.org/10.1016/j.microrel.2016.12.016
[27] T. Matsuoka, E. Kobayashi, K. Taniguchi, C. Hamaguchi, and S. Sasa, "Temperature Dependence of Electron Mobility in InGaAs/InAlAs Heterostructures," *Japanese J. of Appl. Phys.*, vol. 29, no. Part 1, No. 10, p. 2017, oct 1990.
[28] H. Rodilla, J. Schleeh, P.-A. Nilsson, N. Wadefalk, J. Mateos, and J. Grahn, "Cryogenic performance of low-noise InP HEMTs: A Monte Carlo study," *IEEE Trans. Electron Devices*, vol. 60, p. 1625, 05 2013.
[29] S. M. Sze and K. K. Ng, *Physics of Semiconductor Devices*. Wiley-Blackwell, 2007.
[30] M. Singh, Y. R. Wu, and J. Singh, "Velocity overshoot effects and scaling issues in iii-v nitrides," *IEEE Trans. Electron Devices*, vol. 52, p. 311, 3 2005.
[31] M. Farahmand, C. Garetto, E. Bellotti, K. F. Brennan, M. Goano, E. Ghillino, G. Ghione, J. D. Albrecht, and P. P. Ruden, "Monte Carlo simulation of electron transport in the III-nitride wurtzite phase materials system: binaries and ternaries," *IEEE Trans. Electron Devices*, vol. 48, no. 3, p. 535, 2001.
[32] M. Li and Y. Wang, "2-D Analytical Model for Current–Voltage Characteristics and Transconductance of AlGaN/GaN MODFETs," *IEEE Trans. Electron Devices*, vol. 55, no. 1, p. 261, 2008.
[33] Y. G. Xie, S. Kasai, H. Takahashi, C. Jiang, and H. Hasegawa, "Fabrication and characterization of InGaAs/InAlAs insulated gate pseudomorphic HEMTs having a silicon interface control layer," *IEICE Trans. Electronics*, vol. E84-C, no. 10, p. 1335, 2001.
[34] T. Chidambaram, D. Veksler, S. Madisetti, A. Greene, M. Yakimov, V. Tokranov, R. Hill, and S. Oktyabrsky, "Interface trap density and mobility extraction in InGaAs buried quantum well metal-oxide-semiconductor field-effect-transistors by gated Hall method," *Appl. Phys. Lett.*, vol. 104, no. 13, p. 131605, 2014.
[35] M. A. Negara, D. Veksler, J. Huang, G. Ghibaudo, P. K. Hurley, G. Bersuker, N. Goel, and P. Kirsch, "Analysis of effective mobility and hall effect mobility in high-k based $In_{0.75}Ga_{0.25}As$ metal-oxide-semiconductor high-electron-mobility transistors," *Appl. Phys. Lett.*, vol. 99, no. 23, p. 232101, 2011.
[36] A. Sonnet, R. Galatage, P. Hurley, E. Pelucchi, K. Thomas, A. Gocalinska, J. Huang, N. Goel, G. Bersuker, W. Kirk, C. Hinkle, and E. Vogel, "Remote phonon and surface roughness limited universal electron mobility of $In_{0.53}Ga_{0.47}As$ surface channel MOSFETs," *Microelectronic Engineering*, vol. 88, no. 7, pp. 1083–1086, 2011, proceedings of the 17th Biennial International Insulating Films on Semiconductor Conference. [Online]. Available: https://www.sciencedirect.com/science/article/pii/S0167931711003790
[37] H. Zhao, Y.-T. Chen, J. H. Yum, Y. Wang, N. Goel, and J. C. Lee, "High performance In0.7Ga0.3As metal-oxide-semiconductor transistors with mobility >4400 cm^2/Vs using InP barrier layer," *Appl. Phys. Lett.*, vol. 94, no. 19, p. 193502, 2009.
[38] H. Zhao, Y.-T. Chen, J. H. Yum, Y. Wang, F. Zhou, F. Xue, and J. C. Lee, "Effects of barrier layers on device performance of high mobility $In_{0.7}Ga_{0.3}As$ metal-oxide-semiconductor field-effect-transistors," *Appl. Phys. Lett.*, vol. 96, no. 10, p. 102101, 2010.
[39] T. Li, *Ensemble Monte Carlo Based Simulation Analysis of GaN HEMTs for High-Power Microwave Device Applications*. Doctor of Philosophy (PhD), dissertation, Electrical/Computer Engineering, Old Dominion University, 2001.
[40] T. Ando, A. B. Fowler, and F. Stern, "Electronic properties of two-dimensional systems," *Rev. Mod. Phys.*, vol. 54, pp. 437–672, Apr 1982. [Online]. Available: https://link.aps.org/doi/10.1103/RevModPhys.54.437
[41] F. Stern and W. E. Howard, "Properties of semiconductor surface inversion layers in the electric quantum limit," *Phys. Rev.*, vol. 163, pp. 816–835, Nov 1967. [Online]. Available: https://link.aps.org/doi/10.1103/PhysRev.163.816
[42] F. Stern, "Crc critical rev." *Solid State Science*, vol. 499, 1974.
[43] F. Schwierz, "Graphene transistors: Status, prospects, and problems," *Proceedings of the IEEE*, vol. 101, no. 7, p. 1567, 2013.